

Thionated Perylene Diimides with Intense Absorbance in the Near-IR**

Ben A. Llewellyn, E. Stephen Davies, Constance R. Pfeiffer, Mick Cooper, William Lewis and Neil R. Champness*

Supporting Information Table of Contents

Experimental Details	Page 1
UV-vis Spectra of Different redox states of 1	Page 4-5
UV-vis Spectra of Different redox states of 2	Page 5-8
Electrochemical Measurements for 2 in CH ₂ Cl ₂	Page 8-10
EPR spectra of reduced species of 1 and 2	Page 11
DFT Geometry Optimized Structures of 1 and 2	Page 12
Single crystal structure of 4	Page 12

Further Experimental Details

Synthesis of *N,N'*-di(*n*-butyl)-1,7-dimorpholino-3,4:9,10-perylenetetraathio diimide

N,N'-di(*n*-butyl)-1,7-dimorpholino-3,4:9,10-perylenetetracarboxylic acid diimide (1000 mg, 1.49 mmol) and Lawesson's Reagent (3600 mg, 8.91 mmol) were dissolved in dry toluene (200 mL) and heated to reflux for two days under an inert atmosphere. The solution was cooled to room temperature and poured into NaOH (100 mM) and the organic extract was washed with water three times. The solution was dried over MgSO₄ and the solvent was removed under reduced pressure. The crude product was purified by column chromatography (SiO₂, chloroform:EtOAc 97:3) to give the pure product as a dark purple powder (175 mg, 0.237 mmol, 16%). ¹H NMR (CDCl₃/TFA-d, 400 MHz): δ = 9.18 (d, *J*=8.5 Hz, 2 H), 8.57 (d, *J*=8.8 Hz, 2 H), 8.38 (s, 2 H), 5.21 - 5.44 (m, 4 H), 3.85 - 4.14 (m, 8 H), 3.02 - 3.32 (m, 8 H), 1.82 - 2.04 (m, 4 H), 1.55 (sxt, *J*=7.4 Hz, 4 H), 1.08 ppm (t, *J*=7.3 Hz, 6 H); ¹³C NMR (CDCl₃/TFA-d, 126 MHz): δ = 187.3, 149.3, 134.9, 133.3, 128.8, 128.8, 128.3, 127.4, 123.8, 121.8, 119.4, 66.4, 55.6, 51.5, 27.5, 20.1, 13.8 ppm; MS (MALDI-TOF, DCTB matrix, positive mode) Calc: 736.2034 (M⁺) Found: 736.2016 (M⁺).

Synthesis of *N,N'*-di(*n*-butyl)-1,6-dimorpholino-3,4:9,10-perylenetetraathio diimide

N,N'-di(*n*-butyl)-1,6-dimorpholino-3,4:9,10-perylenetetracarboxylic acid diimide (445 mg, 0.661 mmol) and Lawesson's Reagent (1600 mg, 3.96 mmol) were dissolved in dry toluene (100 mL) and heated to reflux for two days under an inert atmosphere. The solution was cooled to room temperature and poured into NaOH (100 mM), and the organic extract was washed with water three

times. The solution was dried over MgSO_4 and the solvent was removed under reduced pressure. The crude product was purified by column chromatography (SiO_2 , chloroform:EtOAc 97:3). Any unreacted tri-thionated PDI was re-reacted with 1.5 equivalents of Lawesson's reagent before work up and purification by the above method. Both crops were combined to give the pure product as a black powder (85 mg, 0.115 mmol, 17%). ^1H NMR (CDCl_3 , 400 MHz): δ = 9.71 (d, $J=8.8$ Hz, 2 H), 8.92 (d, $J=8.8$ Hz, 2 H), 8.60 (s, 2 H), 5.25 - 5.43 (m, 4 H), 3.84 - 4.02 (m, 8 H), 3.29 (d, $J=11.8$ Hz, 4 H), 2.96 - 3.11 (m, 4 H), 1.84 - 2.03 (m, 4 H), 1.45 - 1.56 (m, $J=15.4, 7.7, 7.7$ Hz, 4 H), 1.03 (t, $J=7.3$ Hz, 3 H), 1.04 ppm (t, $J=7.4$ Hz, 3 H); ^{13}C NMR (CDCl_3 , 101 MHz): δ = 188.7, 188.1, 151.9, 137.1, 134.6, 130.8, 129.5, 128.1, 127.9, 125.2, 125.1, 123.7, 123.0, 116.8, 66.4, 55.2, 55.0, 51.9, 27.6, 27.5, 20.1, 20.1, 13.8, 13.8 ppm; MS (MALDI-TOF, DCTB matrix, positive mode) Calc: 736.2034 (M^+) Found: 736.2032 (M^+).

Photophysical, Electrochemical and Spectroelectrochemical Measurements

UV/visible absorption spectra were recorded on a Perkin-Elmer Lambda 25 spectrometer.

Cyclic voltammetric and coulometric studies were carried out using an Autolab PGSTAT20 potentiostat. Standard cyclic voltammetry was carried out under an atmosphere of argon using a three-electrode arrangement in a single compartment cell. A glassy carbon working electrode, a Pt wire secondary electrode and a saturated calomel reference electrode, chemically isolated from the test solution via a bridge tube containing electrolyte solution and fitted with a porous vycor frit, were used in the cell. The solutions were 10^{-3} M in test compound and 0.4 M in $[\text{NBu}_4][\text{BF}_4]$ as supporting electrolyte. Redox potentials are quoted versus the ferrocenium–ferrocene couple used as an internal reference. Compensation for internal resistance was not applied.

Bulk electrolysis experiments, at a controlled potential, were carried out using a two-compartment cell. The Pt/Rh gauze basket working electrode was separated from the wound Pt/Rh gauze secondary electrode by a glass frit. A saturated calomel reference electrode was bridged to the test solution through a vycor frit orientated at the centre of the working electrode. The working electrode compartment was fitted with a magnetic stirrer bar and the test solution was stirred rapidly during electrolysis. The solutions used were 0.4 M in $[\text{NBu}_4][\text{BF}_4]$ as supporting electrolyte and 10^{-3} M in test compound and were prepared using Schlenk line techniques. Electrolysed solutions were transferred to quartz tubes, via teflon canula, for analysis by EPR spectroscopy. EPR spectra were recorded on a Bruker EMX spectrometer.

The UV/vis spectroelectrochemical experiments were carried out with an optically transparent electrochemical (OTE) cell (modified quartz cuvette, optical pathlength: 0.5 mm). A three-electrode configuration, consisting a Pt/Rh gauze working electrode, a Pt wire secondary electrode (in a fritted PTFE sleeve) and a saturated calomel electrode, chemically isolated from the test solution via a bridge tube containing electrolyte solution and terminated in a porous frit, was used in the cell. The potential at the working electrode was controlled by a Sycopel Scientific Ltd DD10M potentiostat. The UV/vis spectra were recorded on a Perkin Elmer Lambda 16 spectrophotometer. The cavity was purged with dinitrogen and temperature control at the sample was achieved by flowing cooled dinitrogen across the surface of the cell. For UV/vis/NIR measurements the reduced species were generated in the same way and the spectra were recorded on a Perkin-Elmer Lambda 750 spectrometer.

Single Crystal X-Ray Diffraction Studies

Single crystal diffraction data on **1** and **2** were collected at 120(2) K on a Bruker GV1000 spectrometer using mirror monochromated Cu K α radiation. For the single crystal structure of **1** disordered solvent chloroform could not be reasonably modelled to give convergence and the data was processed using SQUEEZE.⁵¹ For both structures, **1** and **2**, disorder was observed in the butyl chains of the PDI, appropriate restraints were applied to the thermal parameters of these atoms.

Crystal data for **1**: C₄₀H₄₀N₄O₂S₄. Triclinic, space group *P*-1, $a = 12.8268(14)$, $b = 13.2644(13)$, $c = 24.5245(7)$ Å, $\alpha = 96.008(5)$, $\beta = 95.267(6)$, $\gamma = 118.650(11)^\circ$, $V = 3593.1(6)$ Å³, $Z = 4$, $D_{\text{calc}} = 1.473$ g cm⁻³, $\mu = 3.81$ mm⁻¹, $F(000) = 1668$. A total of 28315 reflections were collected, of which 14170 were unique, with $R_{\text{int}} = 0.133$. Final $R_1 (wR_2) = 0.149 (0.416)$ with GOF = 1.26.

Crystal data for **2**: C₄₀H₄₀N₄O₂S₄·CHCl₃. Triclinic, space group *P*-1, $a = 10.5929(5)$, $b = 13.3915(8)$, $c = 15.0416(8)$ Å, $\alpha = 93.393(5)$, $\beta = 105.711(5)$, $\gamma = 107.519(5)^\circ$, $V = 1935.59(19)$ Å³, $Z = 2$, $D_{\text{calc}} = 1.469$ g cm⁻³, $\mu = 4.51$ mm⁻¹, $F(000) = 892$. A total of 14080 reflections were collected, of which 7626 were unique, with $R_{\text{int}} = 0.051$. Final $R_1 (wR_2) = 0.061 (0.166)$ with GOF = 1.02.

Crystal data for **4**: C₄₀H₄₀N₄O₆·CHCl₃. Monoclinic, space group *P*2₁/*c*, $a = 12.7735(2)$, $b = 8.38150(10)$, $c = 32.1723(5)$ Å, $\beta = 111.6840(10)^\circ$, $V = 3200.66(8)$ Å³, $Z = 4$, $D_{\text{calc}} = 1.396$ g cm⁻³, $\mu = 0.767$ mm⁻¹, $F(000) = 1424$. A total of 12505 reflections were collected, of which 6283 were unique, with $R_{\text{int}} = 0.016$. Final $R_1 (wR_2) = 0.0436 (0.1269)$ with GOF = 1.04.

DFT Calculations

DFT calculations were carried out using the B3LYP/6-31G* basis set. The geometry optimized structures showed the expected twist in the perylene core due to the steric bulk of the morpholine.

The LUMO energies of **1** and **2** were calculated as -3.75 eV and -3.76 eV respectively, consistent with the first reduction potentials being almost identical. This result matches that of **3** and **4** which were also found to be identical. The HOMO energy levels were calculated as -5.273 eV for **1** and -5.309 eV for **2**, a difference of 0.036 eV. The 1,6- isomer having a lower HOMO energy than the 1,7- isomer is in keeping with the measurements for **3** and **4**. The molecular orbital diagrams for **1** (see below) show the HOMO and the LUMO to be a similar shape to the equivalent diagrams for **3** but with more electron density lying on the sulphur atoms. The molecular orbital diagrams of **2** show the electron density mainly lies around the naphthalene ring bearing the morpholine subunits in the LUMO but in the HOMO the electron density is mainly on the unsubstituted naphthalene ring. All calculations were performed with Gaussian 03 Revision D. 01.^{S2}

Supplementary Figures

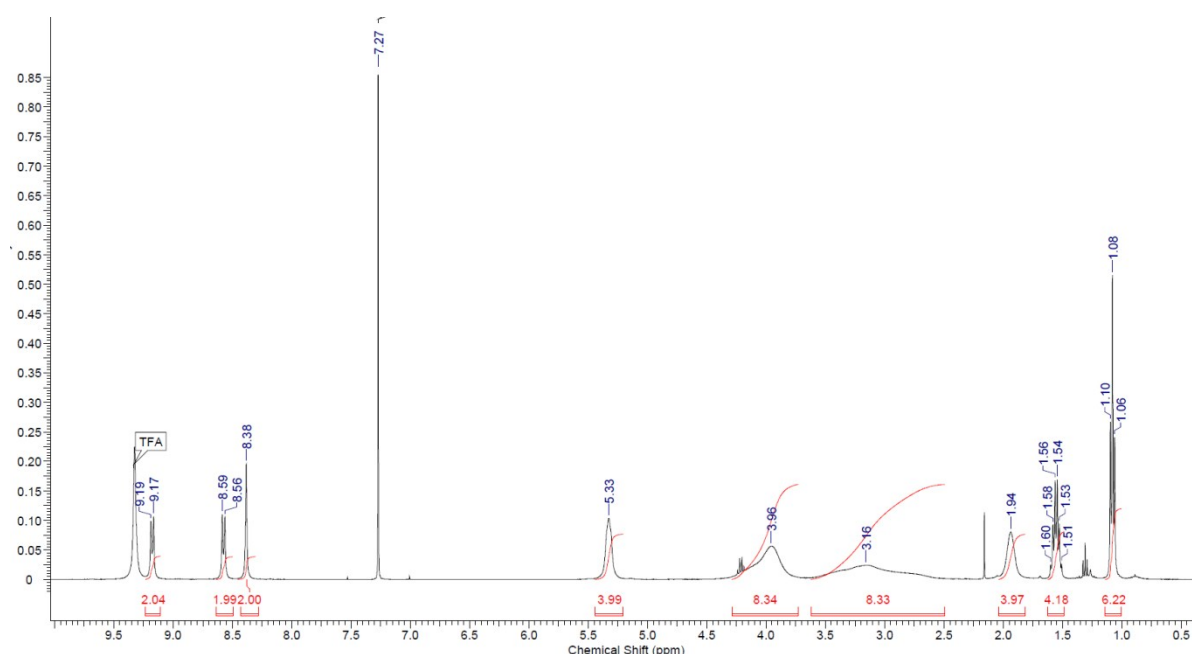


Fig. S1 ¹H NMR spectrum for **1** recorded in CDCl₃ solution.

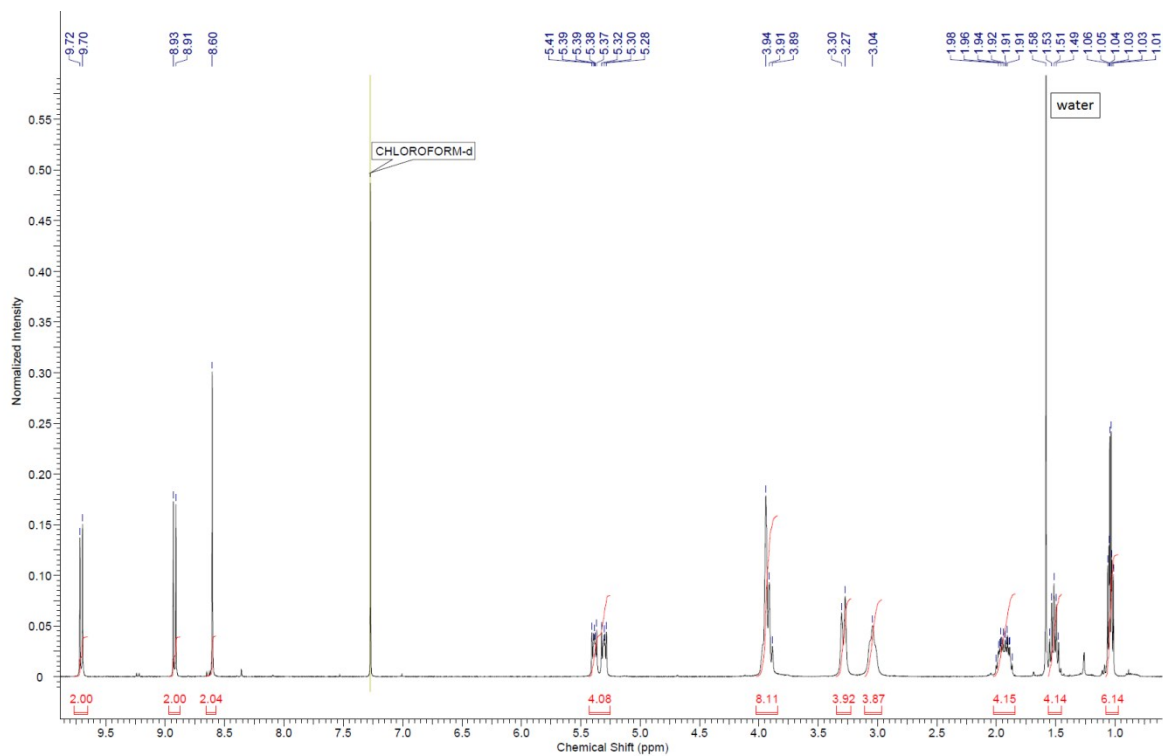


Fig. S2 ^1H NMR spectrum for **2** recorded in CDCl_3 solution. A peak corresponding to H_2O was always observed despite prolonged drying of the sample.

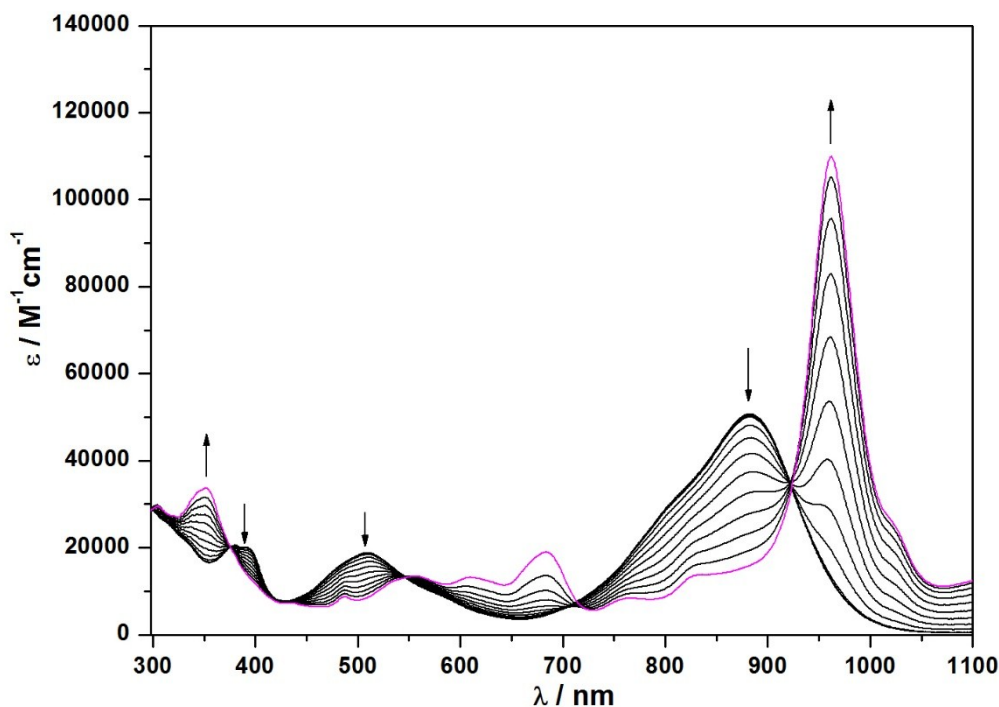


Fig. S3 View of UV-visible spectra recorded in 1,2-dichlorobenzene containing $[\text{Bu}_4\text{N}][\text{BF}_4]$ (0.4 M) using spectroelectrochemical methods for **1** at 273 K showing the inter-conversion of **1** to **1 \cdot** . Arrows indicate the progress of the reduction.

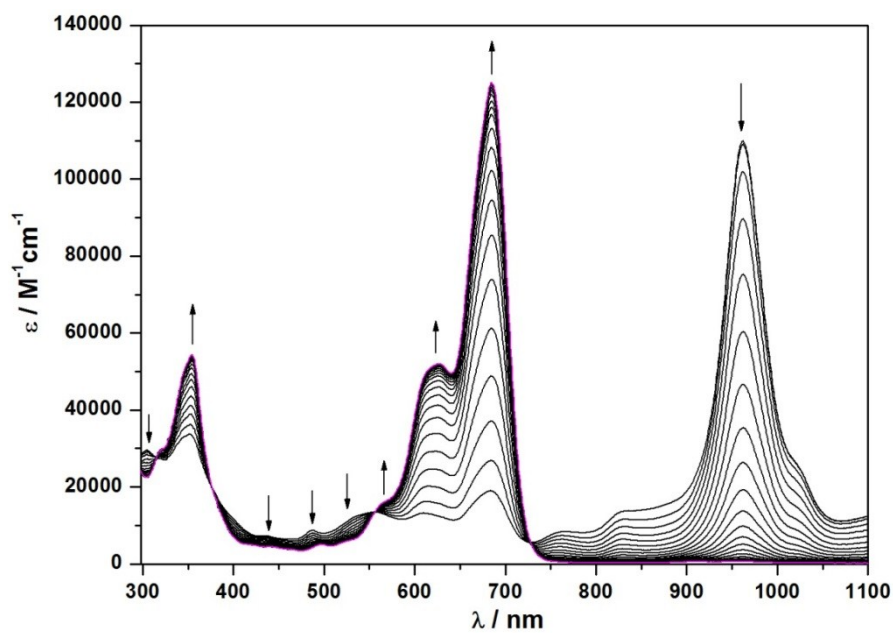


Fig. S4 View of UV-visible spectra recorded in 1,2-dichlorobenzene containing $[\text{Bu}_4\text{N}][\text{BF}_4]$ (0.4 M) using spectroelectrochemical methods for **1** at 273 K showing the inter-conversion of **1**⁻ to **1**²⁻. Arrows indicate the progress of the reduction.

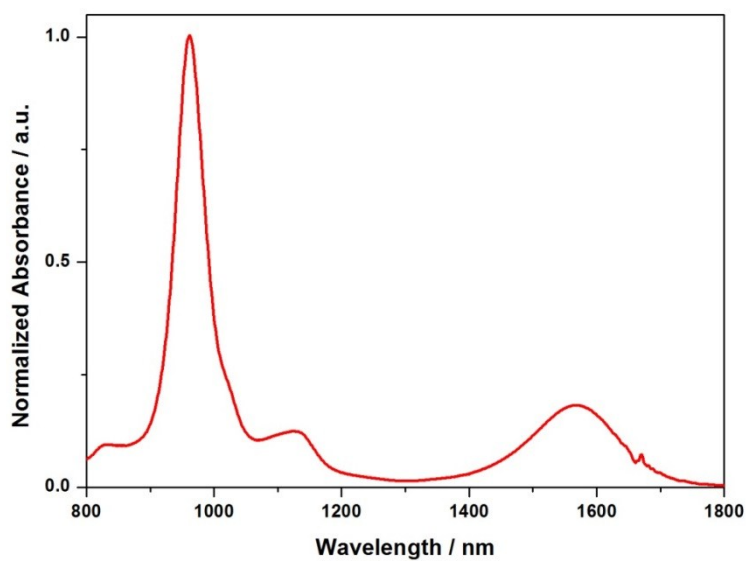


Fig. S5 UV-visible spectra of **1**⁻ recorded in DCB.

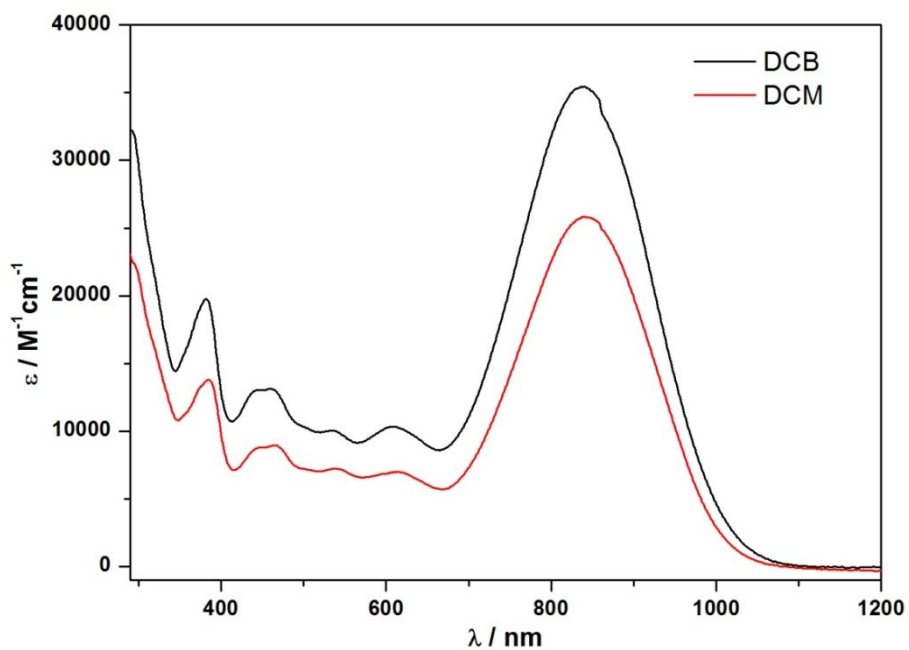


Fig. S6 UV-visible spectra of **2** recorded in CH_2Cl_2 (red line) and 1,2-dichlorobenzene, (black line).

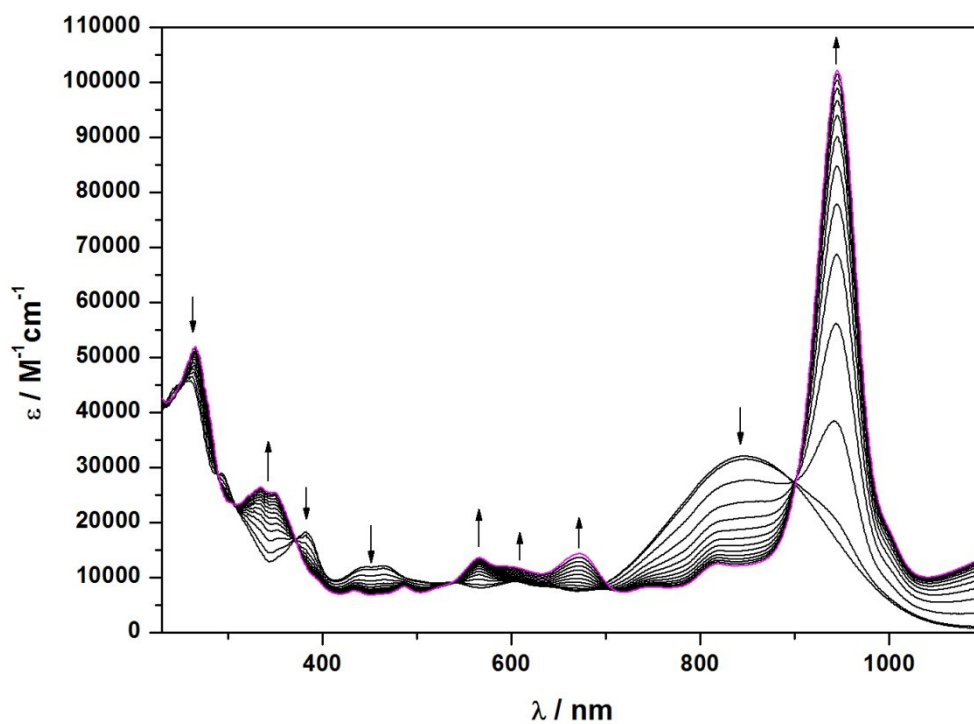


Fig. S7 View of UV-visible spectra recorded in CH_2Cl_2 containing $[\text{Bu}_4\text{N}][\text{BF}_4]$ (0.4 M) using spectroelectrochemical methods for **2** at 273 K showing the inter-conversion of **2** to **2 \cdot^-** . Arrows indicate the progress of the reduction.

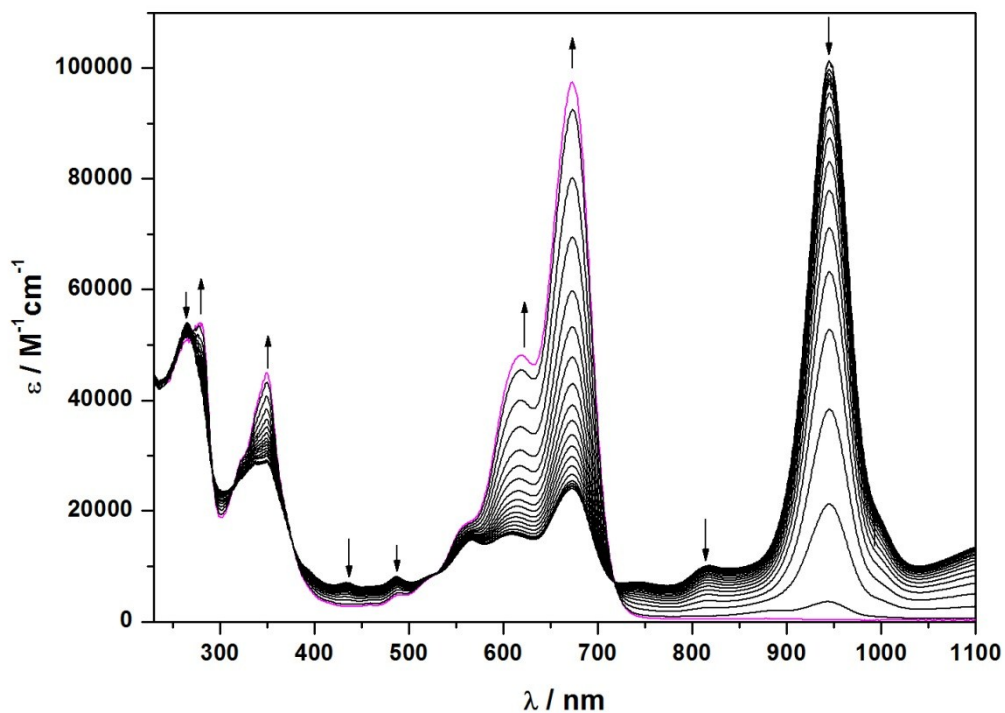


Fig. S8 View of UV-visible spectra recorded in CH_2Cl_2 containing $[\text{Bu}_4\text{N}][\text{BF}_4]$ (0.4 M) using spectroelectrochemical methods for **2** at 273 K showing the inter-conversion of **2** to **2²⁻**. Arrows indicate the progress of the reduction.

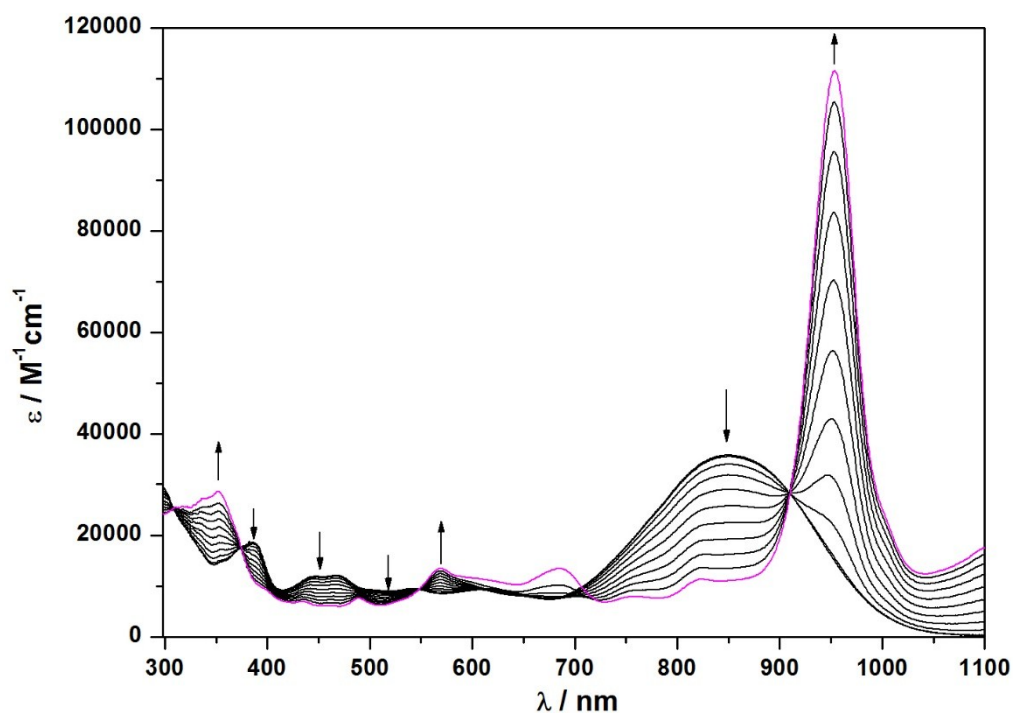


Fig. S9 View of UV-visible spectra recorded in 1,2-dichlorobenzene containing $[\text{Bu}_4\text{N}][\text{BF}_4]$ (0.4 M) using spectroelectrochemical methods for **2** at 273 K showing the inter-conversion of **2** to **2⁻**. Arrows indicate the progress of the reduction.

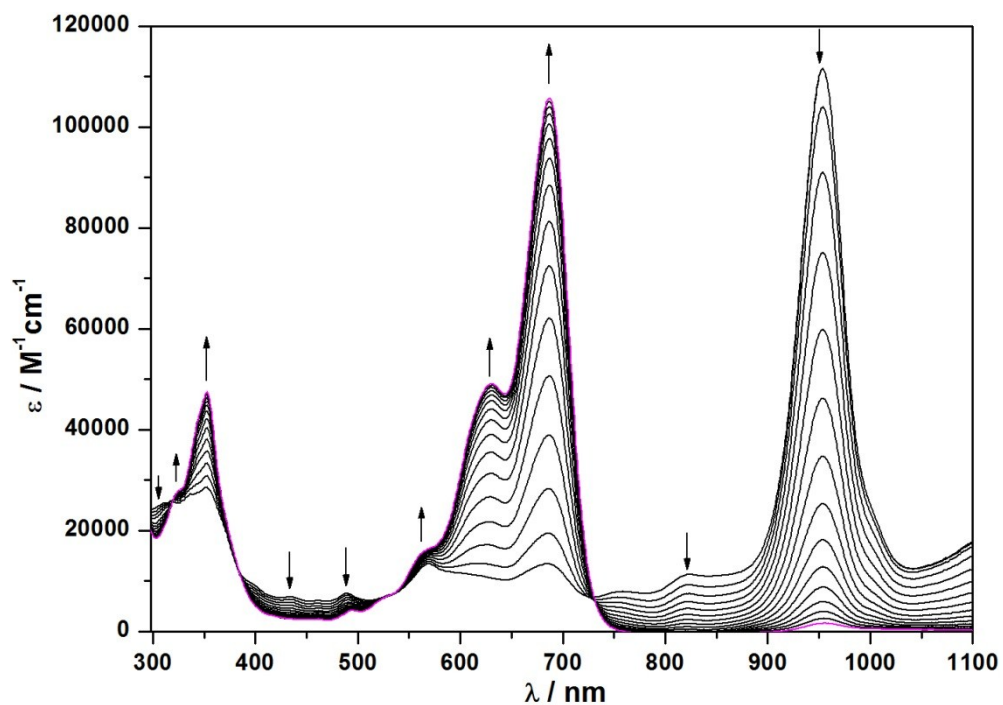


Fig. S10 View of UV-visible spectra recorded in 1,2-dichlorobenzene containing $[\text{Bu}_4\text{N}][\text{BF}_4]$ (0.4 M) using spectroelectrochemical methods for **2** at 273 K showing the inter-conversion of 2^- to 2^{2-} . Arrows indicate the progress of the reduction.

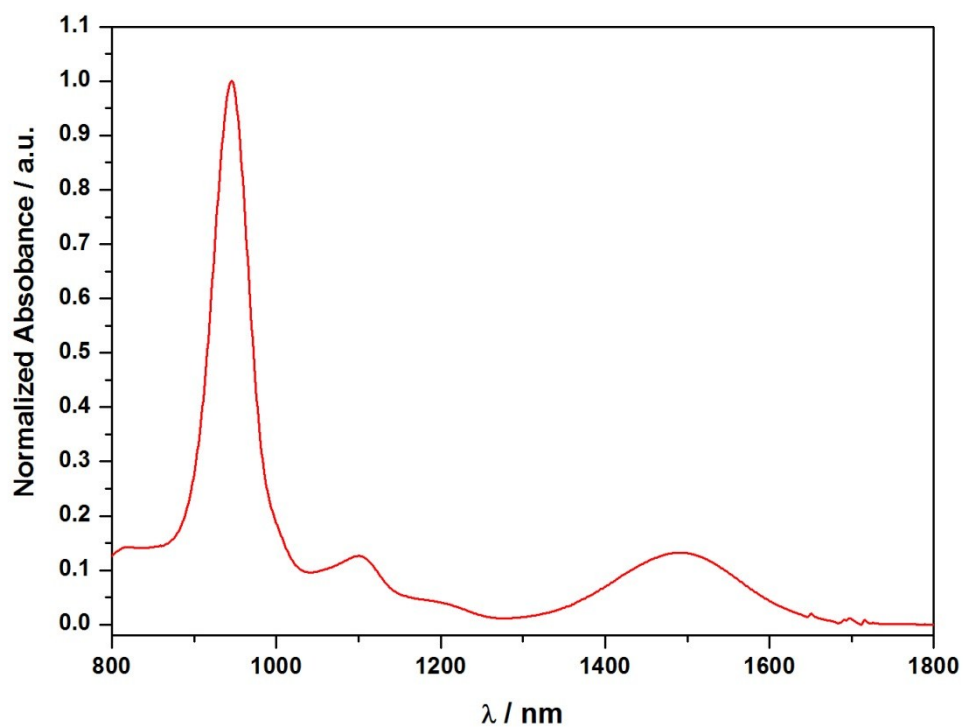


Fig. S11. UV-visible spectra of 2^- recorded in 1,2-dichlorobenzene.

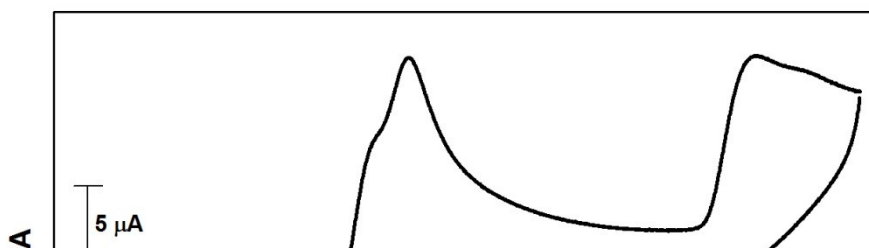


Fig. S12. Cyclic voltammogram recorded for **2** in CH₂Cl₂ containing [Bu₄N][BF₄] (0.4 M) .

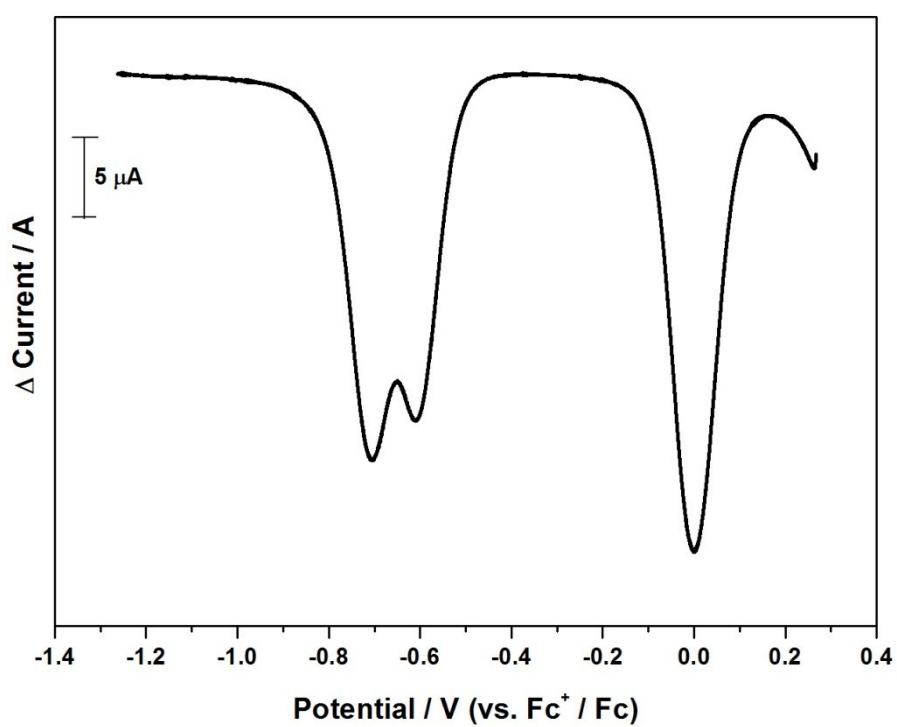


Fig. S13. Square wave voltammogram recorded in CH₂Cl₂ containing [Bu₄N][BF₄] (0.4 M) for **2**.

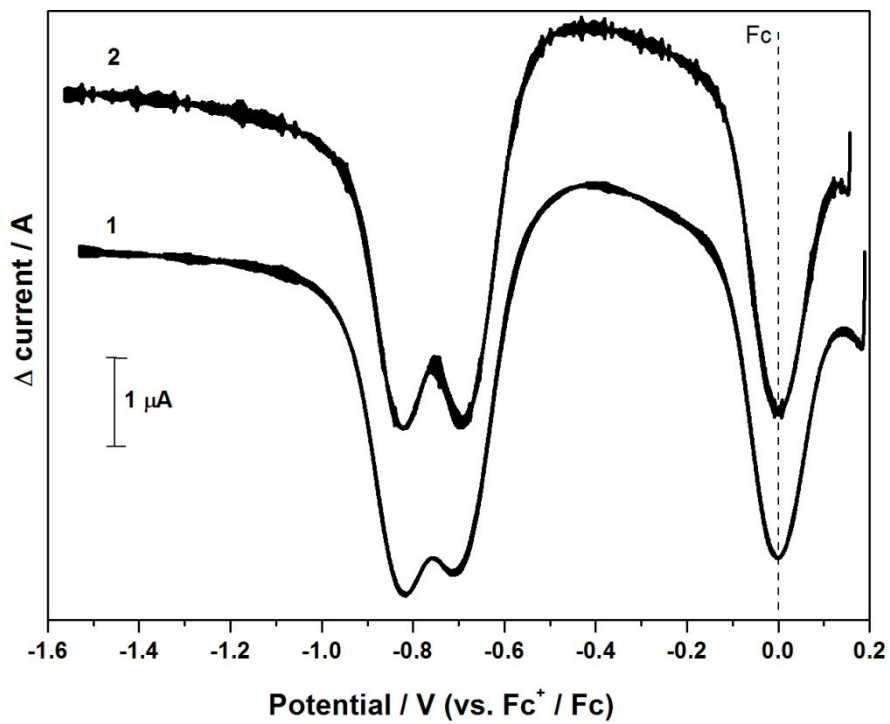


Fig. S14. Comparison of square wave voltammograms recorded in 1,2-dichlorobenzene for **1** and **2**.

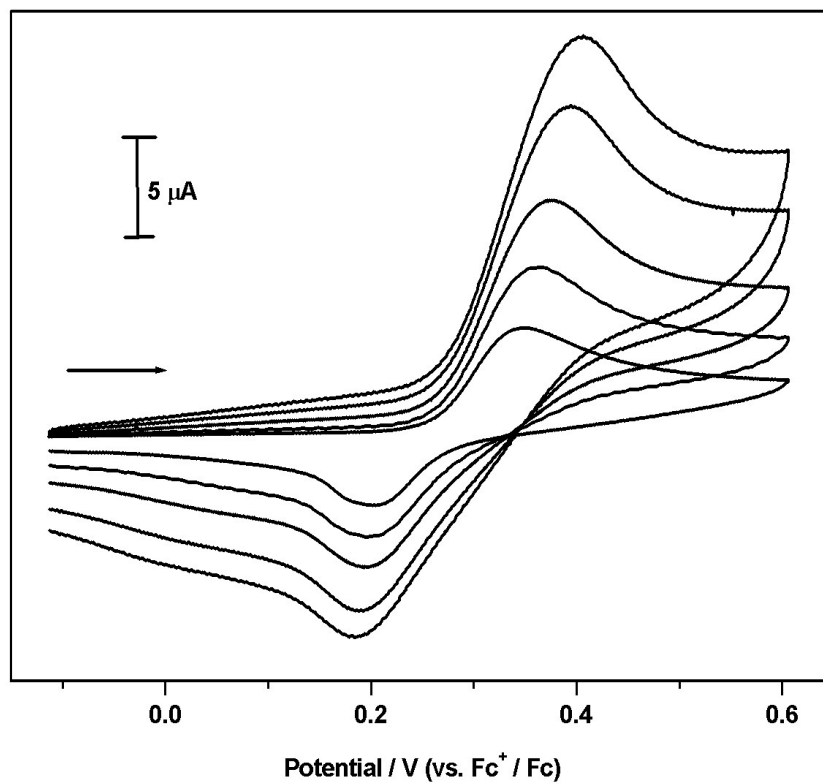


Fig. S15. Cyclic voltammetry for **1**, showing the oxidative process, recorded in 1,2-dichlorobenzene containing $[\text{Bu}_4\text{N}][\text{BF}_4]$ (0.4 M) at scan rates of 0.02, 0.05, 0.1, 0.2 and 0.3 Vs^{-1}

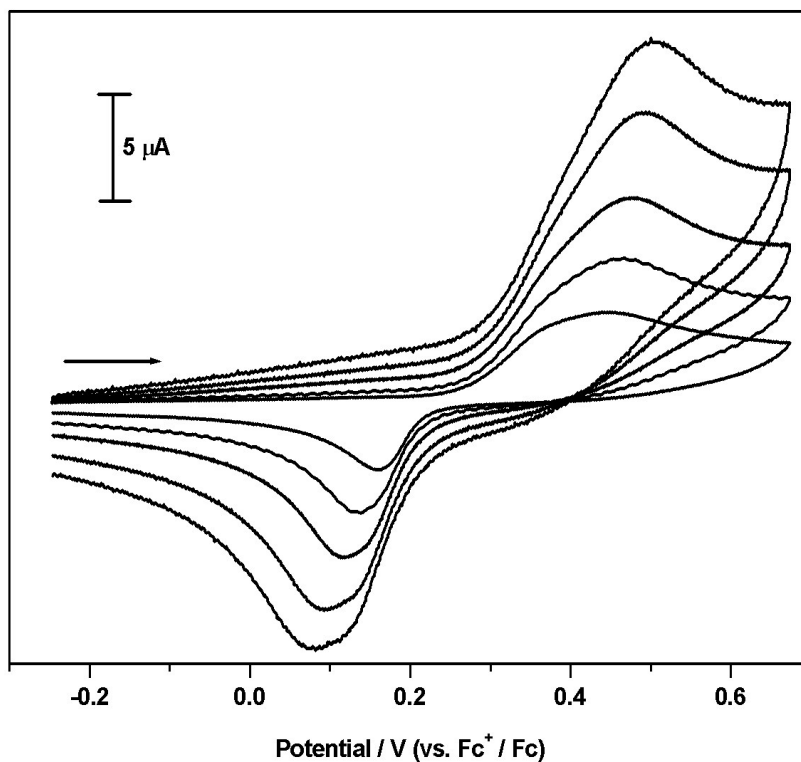


Fig. S16. Cyclic voltammetry for **2**, showing the oxidative process, recorded in 1,2-dichlorobenzene containing $[\text{Bu}_4\text{N}][\text{BF}_4]$ (0.4 M) at scan rates of 0.02, 0.05, 0.1, 0.2 and 0.3 Vs^{-1}

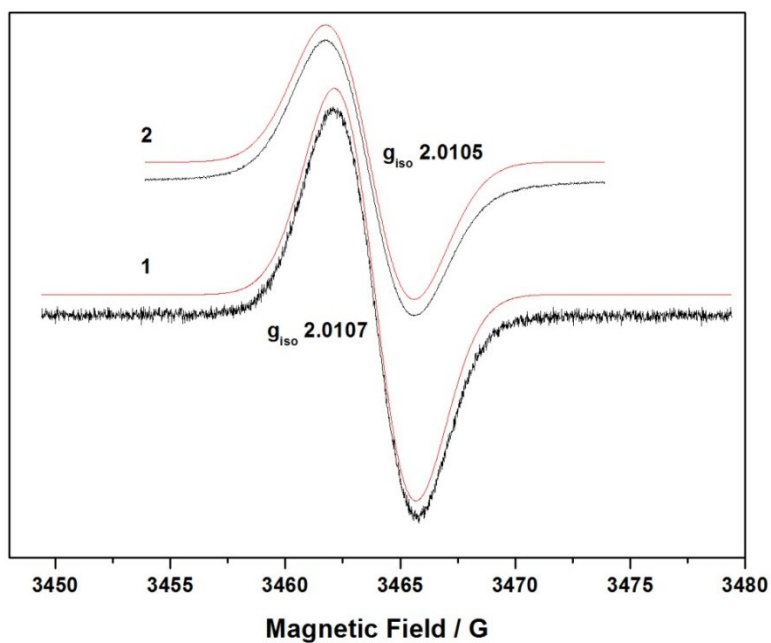


Fig. S17. Comparison of EPR spectra recorded for **1** and **2**, simulated spectra are shown in red.

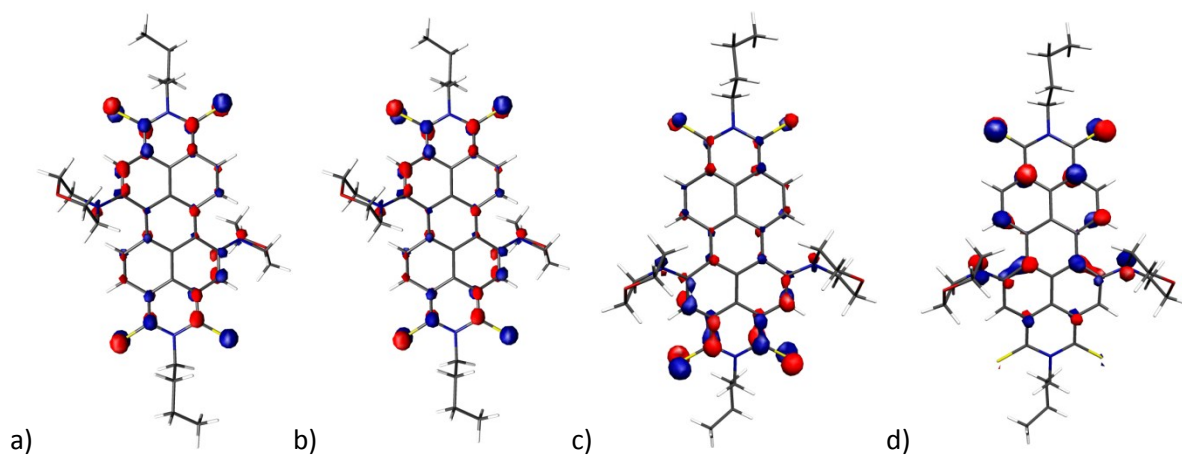


Fig. S18. The isosurfaces at $0.04 \text{ e}\text{\AA}^{-3}$ for the (a) LUMO of **1**; (b) HOMO of **1**; (c) LUMO of **2**; (d) HOMO of **2**.

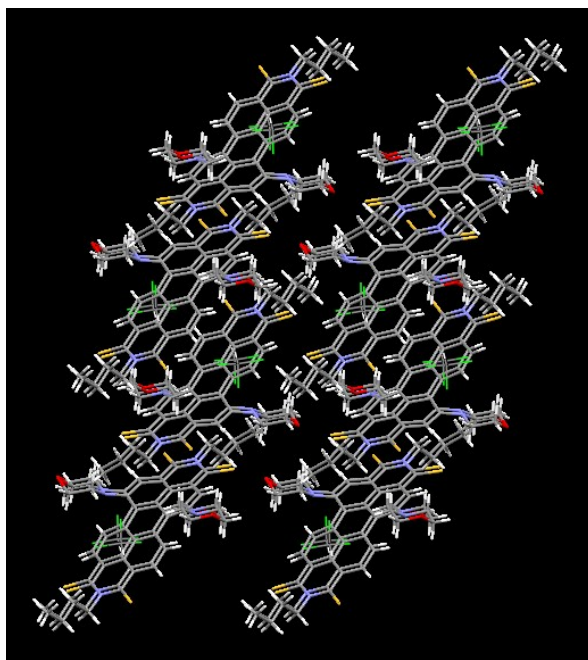


Fig. S19. View of the packing in the single crystal structure of **2**·CHCl₃ along the crystallographic a-axis Carbon- grey, nitrogen- blue, oxygen- red, hydrogen – white, chlorine - green.

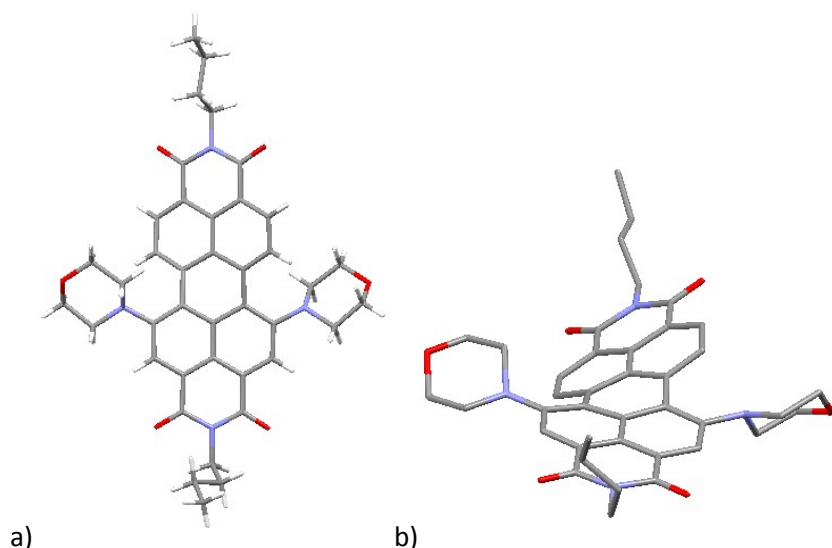


Fig. S20. Views of the single crystal structure of **4**, showing (a) the 1,6 substitution of the perylene core; b) illustrating the twist of the perylene core as a result of bay-region substitution. Carbon- grey, nitrogen- blue, oxygen- red, hydrogen - white. In b) H-atoms are removed for clarity.

Reference

- S1. a) P. v der Sluis, A. L. Spek, *Acta Crystallogr. Sect. A*, 1990, **46**, 194; b) A.L. Spek, *Acta Crystallogr., Sect. D*, 2009, **65**, 148-155.
- S2. Frisch, M. J.; Trucks, G. W.; Schlegel, H. B.; Scuseria, G. E.; Robb, M. A.; Cheeseman, J. R.; Zakrzewski, V. G.; Montgomery, J. A.; Stratmann, R. E.; Burant, J. C.; Dapprich, S.; Millam, J. M.; Daniels, A. D.; Kudin, K. N.; Strain, M. C.; Farkas, O.; Tomasi, J.; Barone, V.; Cossi, M.; Cammi, R.; Mennucci, B.; Pomelli, C.; Adamo, C.; Clifford, S.; Ochterski, J.; Petersson, G. A.; Ayala, P. Y.; Cui, Q.; Morokuma, K.; Malick, D. K.; Rabuck, A. D.; Raghavachari, K.; Foresman, J. B.; Cioslowski, J.; Ortiz, J. V.; Stefanov, B. B.; Liu, G.; Liashenko, A.; Piskorz, P.; Komaromi, I.; Gomperts, G.; Martin, R. L.; Fox, D. J.; Keith, T.; Al-Laham, M. A.; Peng, C. Y.; Nanayakkara, A.; Gonzalez, C.; Challacombe, M.; Gill, P. M. W.; Johnson, B. G.; Chen, W.; Wong, M. W.; Andres, J. L.; Head-Gordon, M.; Replogle, E. S.; Pople, J. A. *Gaussian 03 Revision D. 01*; Gaussian, Inc., Wallingford CT, 2004.